IEEE Access
Multidisciplinary | Rapid Review | Open Access Journal

Received February 13, 2019, accepted February 25, 2019, date of publication March 25, 2019, date of current version June 4, 2019.

*Digital Object Identifier 10.1109/ACCESS.2019.2902168*

# Quantitative Cone-Beam CT Imaging in Radiotherapy: Parallel Computation and Comprehensive Evaluation on the TrueBeam System

**XIAOKUN LIANG[1,2], YANGKANG JIANG[3,4], YAOQIN XIE[1], AND TIANYE NIU[3,4]**

[1]Shenzhen Institutes of Advanced Technology, Chinese Academy of Sciences, Shenzhen 518055, China
[2]Shenzhen College of Advanced Technology, University of Chinese Academy of Sciences, Shenzhen 518055, China
[3]Sir Run Run Shaw Hospital, Zhejiang University School of Medicine, Hangzhou 310016, China
[4]Institute of Translational Medicine, Zhejiang University, Hangzhou 310016, China

Corresponding author: Tianye Niu (tyniu@zju.edu.cn)

This work was supported in part by the Zhejiang Provincial Natural Science Foundation of China under Grant LR16F010001, Grant LY16H180001, and Grant LY17E050008, in part by the National High-tech R&D Program for Young Scientists by the Ministry of Science and Technology of China under Grant 2015AA020917, in part by the National Key Research Plan by the Ministry of Science and Technology of China under Grant 2016YFC0104507 and Grant 2016YFC0105102, in part by the Natural Science Foundation of China under NSFC Grant 81871351, Grant 81201091, and Grant 51305257, in part by the Zhejiang Province 151 Talents Program, in part by the Zhejiang University Education Foundation ZJU-Stanford Collaboration Fund, and in part by the Opening Fund of Engineering Research Center of Cognitive Healthcare of Zhejiang Province.

**ABSTRACT** Cone-beam CT (CBCT) imaging is used in the patient setup on the advance image-guided radiation therapy. However, the scatter contamination causes spatial non-uniformity, the error of the CT number, and image contrast loss, which is considered as one of the fundamental limitations for CBCT application. In this paper, we use both scatter correction and noise suppression for improving the quality of CBCT image and comprehensively evaluate our method on patient data. A CBCT software package with parallel computation is designed, which is easily compatible with the existing CBCT system of radiotherapy device with high computing efficiency and CT number accuracy. The primary signals of projections are estimated through the use of the forward projections from the registered planning CT (pCT). The errors of low frequency in the raw projections are obtained through subtracting the forward projections and the low-pass filter implementation. The penalty-weighted-least-square (PWLS) method is applied to reduce the high-frequency noise in the corrected CBCT projections. We use the graphics-processing unit (GPU) NVidia Tesla C2075 card with CUDA C programming to accelerate the time-consuming processes. The CBCT projections of a pelvis phantom and the two pelvis patients are obtained from the Varian TrueBeam system, which is a machine for the radiotherapy. The maximum errors of CT number are reduced over 70 HU on the TrueBeam result to below 15 HU, and the errors of spatial non-uniformity are decreased by a factor of around 7. The computation time is about 25 min on the GPU, which is reduced over 10 h on the CPU. The proposed software shows superior performance over the existing reconstruction. The proposed software demonstrates the reliability of the high-accuracy CBCT-based image-guided radiotherapy (IGRT), providing the high-precise CBCT with less computation time.

**INDEX TERMS** Quantitative cone-beam CT, scatter correction, GPU, planning CT, radiotherapy.

## I. INTRODUCTION

Cone-beam CT (CBCT) is important in the modern radiation therapy due to its on-board imaging capability [1], [2]. However, scatter contamination from a large cone angle of CBCT leads to inferior image qualities [3], [4], and the CBCT applications are mainly limited to patient setup [5], [6]. Recently, a shading correction algorithm was proposed using the planning CT (pCT) as the prior to obtain a high quality CBCT [7], [8]. In general, the corrected projections are

The associate editor coordinating the review of this manuscript and approving it for publication was Yi Zhang.

inevitable to remain the scatter noise with high-frequency, and it deteriorates the detail of the image. Another algorithm is also proposed to suppress the increased noise by using the penalty-weighted-least-square (PWLS) algorithm [9]. In this paper, we combine the above two algorithms and comprehensively evaluate the performance on patient data. A software package is designed for quantitative CBCT imaging in a clinical environment. We aim to make the software fully compatible with the protocol of current radiation therapy, to achieve the high accuracy of CT number and improve the spatial uniformity, and to fully accelerate the computation within a time limit of clinical acceptance. The phantom and the patient data obtained on the TrueBeam system (Varian Medical System, Palo Alto, CA, USA) is performed on our software, a state-of-art equipment with several novel techniques already built in to improve CBCT image qualities.

In current radiotherapy, the patients are scanned by diagnostic CT for the purpose of treatment planning. To reduce the patient geometric differences between planning and treatment days, an on-board kV CBCT scanner is mounted on the gantry to visualize the patient's anatomical structures. As such, the on-board patient positions can be aligned well to the geometry on planning day. Since CBCT provides patient anatomical information at treatment time, it plays a vital role in the advanced image-guided radiotherapy (IGRT), including the online contour of the tumor, [10], [11], dose calculation [12]–[14] and adaptive radiation therapy [15], [16]. Nevertheless, these advanced applications are hindered by the inferior image quality of current CBCT [3], [4], [17]. The error comes from several sources during the data acquisition, including scatter contamination [3], beam-hardening effects [18] and etc. Among all the above issues, scatter contamination contributes the majority since the CBCT scanners have a large cone angle [3]. For example, the image error of CBCT due to scatter is up to 300 HU around bony structures on a pelvis patient [8].

Several scatter removal algorithms have been developed in the literatures. Typical examples include several general solutions: analytical modeling [19], primary modulation [20], measurement based methods [21]–[23] and etc. A detailed review can be found in ref. [4]. Though demonstrated effective in certain applications, these general methods fail to fully utilize the available patient information and have limited efficacy in radiotherapy. To expand the clinical use of CBCT, a shading correction algorithm using pCT as a prior information have been proposed and evaluated in our previous study. The results were shown in both phantoms and patient studies [7], [8]. We successfully decreased the overall errors of the CT number from 300 HU to 16 HU [7], [8].

As a general problem, the corrected CBCT projections have the noise of scatter due to its property of high-frequency [9]. The increased noise degrades the image details and lowers the detectibility of low-contrast object [3]. On an anthropomorphic thorax phantom, it has been shown that the radiation dose would be increased by one order of magnitude to maintain the same noise level in CT images as that before correction [9]. To gain from the scatter correction, we have also proposed a noise suppression algorithm applied on the corrected projections and successfully reduced the image noise similar to its original level with no increase of radiation dose [9].

Despite the superior performances, the above two methods are not yet practical in CBCT applications in hospitals mainly due to their time-consuming on the CPU computer. To promote the clinical use of our methods in this work, a useful software package is designed by combining the above two algorithms so that the CBCT correction and reconstruction can be performed in a stream-line fashion. The computation is accelerated on a graphics-processing-unit (GPU) based workstation. GPU is featured by its powerful capability of parallel computation, which is compatible with the calculation structures of our proposed operations. The imaging performance is comprehensively evaluated on both the CBCT of the phantom and the patient data, which is scanned on the on-board imager (OBI) installed on the TrueBeam system.

## II. METHODS

### A. QUANTITATIVE CBCT IMAGING USING THE PLANNING CT AS PRIOR INFORMATION

Fig.1 demonstrates the overall workflow of our software package. Detailed descriptions of each of these steps can be found in our previous publications (see refs. [7] and [8]). Note that the scatter correction component may contain multiple iterations of the listed operations for a better performance as demonstrated in ref. [8]. pCT acquired for the treatment planning is considered as "scatter-free" and registered to the same object in the CBCT (step 2). We use the forward projection operation in the registered pCT image to estimate the primary signals in the CBCT (step 3). The variance (step 4) between the CBCT projections and the estimated primary signals include dominantly low-frequency scatter, [20], [24]–[26] which is accurately estimated using low-pass filtering (step 5). And then we use the raw projections to subtract estimated errors (step 6). The remaining scatter noise is suppressed using PWLS algorithm (step 7) [9] and the corrected CBCT are obtained through the use of a conventional FDK reconstruction algorithm (step 8) [27]. In our previous studies, the whole framework is implemented in Matlab and C using a single CPU core and takes about 10 hours for one iteration.

### B. SCATTER NOISE SUPPRESSION

The algorithm applies a PWLS algorithm to find the optimal approximations to the noisy line integrals after scatter correction via smoothing and edge-preserving formulation [9]. The objective function of PWLS models the first and the second moments of the projection as a weighted least-square (WLS) form and regularizes the WLS term with a penalty to trade off the data fidelity and smoothness:

$$\Phi\left(\hat{q}_c\right) = \left(q_c - \hat{q}_c\right)^T \Sigma^{-1} \left(q_c - \hat{q}_c\right) + \beta R\left(\hat{q}_c\right), \qquad (1)$$

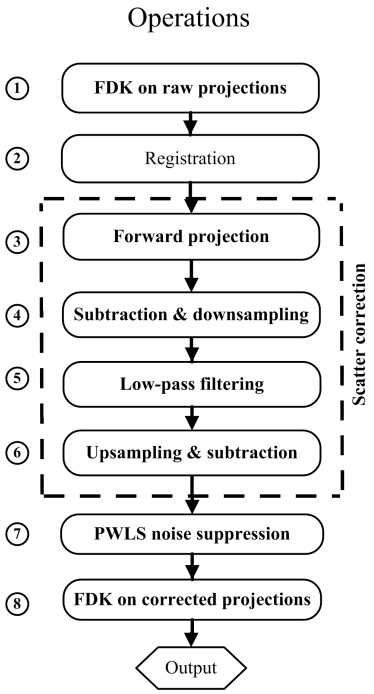


**FIGURE 1.** Diagram of the proposed software package. Note that only one iteration is shown for the scatter correction component.

where $\hat{q}_c$ denotes the vector of the noise-suppressed images of the line integrals which is to be estimated, $q_c$ indicates the vector of noisy line integral image, $\Sigma$ denotes a diagonal matrix whose ith diagonal element is the variance of $q_c$ on the pixel of the detector i. R denotes the penalty function of the smoothness. Based on the Poisson statistics, the variance of $q_c$ can be written as

$$var\,(q_c) \approx \frac{p_m}{(p_m - s_e)^2}, \tag{2}$$

where $p_m$ is the measured the projection image without logarithm and scatter correction. $s_e$ is the estimated scatter. The degree of agreement between the estimated and the measured data are controlled by the parameter $\beta$, and it can determine the smoothness of the result. To minimize the objective, a Gauss-Seidel (GS) solver is used on 2D projection images to iteratively calculate the value of each pixel from its updated neighborhoods.

### C. GPU ACCELERATION

GPU executes multiple and concurrent threads in the processor cores and therefore provides a powerful computation capability [28], [29]. The state-of-the-art GPU cards contain hundreds of computing cores and each core runs at about 1 GHz. Thus the expected highest speedup could be more than 100 times compared to that on a single 3 GHz CPU core [29].

In the scatter correction component of the proposed method, majority of the computation occurs in the CT system modeling (i.e. forward/backward projection) and the image filtering (i.e. pixel-wise median and low-pass filtering). These steps have a structure of parallel processing, readily implementable on GPU. In the forward projection, each GPU thread calculates the weighted summation along one projection line based on Siddon's ray-tracing algorithm [30]. Such a ray-driven scheme is not used in the backprojection process, since it requires random memory access of the voxels and degrades the computation performance. Instead, we apply a voxel-driven scheme where each thread computes the reconstruction voxel value from all the projection views. As a result, all the voxels are updated by the same amount of threads in a concurrent mode. Similar pixel-driven scheme is applied in the median filter design. Each thread operates one pixel in the projection image and picks up the median value of all the pixels constrained by a designed square window.

In our method, the noise suppression is applied on each projection independently. It is worth mentioning that the GS updating scheme used in our current algorithm requires the knowledge of neighboring pixel values to update one pixel. Thus, we employ the projection-driven method where one thread performs the GS iterations over one projection.

### D. THE TRUEBEAM SYSTEM

The TrueBeam system consists of a linear accelerator for radiation therapy treatment and a kV OBI component for patient positioning. The system software incorporates a multitude of innovative techniques for cancer treatment, including imaging, patient positioning, motion management, and treatment delivery.

### E. EVALUATION

#### 1) DATA ACQUISITION

The proposed method was performed on an anthropomorphic pelvis phantom (http://www.supertechx-ray.com) and the two patients. The projections were obtained from the OBI of the TrueBeam system. The mode of scan is in the half-fan scan and 656 projections are obtained with the bowtie filter in a 360 degrees scan. Each projection has the pixel size of $1024\times768$ and the pixel resolution is $0.388\times0.388$ mm2. The reconstructed CBCT volume of our software and TrueBeam has a size of $512 \times 512 \times 81$ with the voxel resolution of $0.91 \times 0.91 \times 1.99$ mm3.

The size of the pCT images are $512 \times 512 \times 94$, and the voxel resolution is 1.27 mm in the direction of axial, and 5 mm in the direction of longitudinal. The phantom was scanned at Emory University Hospital on a 16-slice CT simulator. The two patients, planned for radiotherapy at Peking Cancer Hospital & Institute, were scanned on the CT simulator.

#### 2) IMPLEMENTATION DETAILS

In the implementation, 3D Slicer which is an open-source software is applied (www.slicer.org), for deformable image registration between the pCT and CBCT volumes. In all directions of the image, the size of the grid applied in the deformable registration with B-spline was ten voxels. After 20 iterations, the goal of the optimization was reached. It took 7 minutes for each registration on the desktop.

The other steps used a single TESLA C2075 card installed on an Amax® GPU workstation (www.amax.com). C2075 has 448 processing cores, which are in the clock speed of 1.15 GHz. To use the massive capability of the GPU, we employed CUDA C (NVIDIA, Santa Clara, CA) as the programming environment, which is an extension of the standard C/C++ language with the programming model of single instruction multiple threads. CUDA C is featured with the GPU accelerated libraries to facilitate the program development. In our program, we used the CUDA CUBLAS library to manipulate the vector operations and CUDA CUFFT library to perform the ramp filtering in the FDK reconstruction.

To trade off the computation time and correction performance, only 2 iterations were applied in the scatter correction step to process one data set. In step 3 and 4, a 4-time downsampling on the projection images was applied to reduce the computation time. In step 5, the median filter with $27 \times 27$ pixels in the downsampled projection images (equivalent to $41.9 \times 41.9$ mm$^2$), was applied to reduce the boundary errors in the difference between the estimated projections and the raw projections. The low-pass Gaussian filter ($10.9 \times 10.9$ mm2 on the detector) in the downsampled projection and the 7 pixels (10.9 mm on the detector) of standard deviation, was implemented to decrease the high-frequency difference without changing the low-frequency scatter. Through the use of the beam blocker and the Monte-Carlo simulation which have been published, we estimated the filters' parameters during the sampling of scatter measurement [7], [21], [25]. We suppressed the error in the difference image because of the mis-registered with these parameters. When the width of the filter is in the large range (from 7 pixels to 47 pixels), the proposed method performance is not sensitive to the parameters of the filters. In step 6, the estimated scatter in a coarse grid was upsampled using a bilinear interpolation by 4 times to the full resolution ($1024 \times 768$) before subtracting from the raw projections. In step 7, the penalty weight (i.e., $\beta$ value) of the noise suppression was selected as 0.03 for a spatial resolution close to the Truebeam images.

#### 3) IMAGE QUALITY METRICS

In all the evaluations, the registered pCT images were considered as the reference image. The mean of the CT number value and the spatial non-uniformity (SNU) were calculated for quantitative evaluations of the designed software [8]. The SNU is defined as that in ref [8]:

$$SNU = \frac{\overline{HU}_{\max} - \overline{HU}_{\min}}{1000} \times 100\%, \tag{3}$$

The region of interest (ROI) were chosen in the reconstructed image in the periphery and the center. $\overline{HU}_{min}$ and $\overline{HU}_{max}$ are the minimum and the maximum of the mean of the CT number, respectively.

## III. RESULTS

### A. TIME OF COMPUTATION USING GPU AND CPU

The comparison of CPU and GPU on the computation time performance is listed in Table 1 for major steps shown in Fig. 1. On CPU using Matlab and C, the system modeling (forward/backward projection) costs about 85% of the total computation time. The reason is that the 3D volume has a tremendous amount of voxels ($512 \times 512 \times 200 \approx 107$) and the total number of projection lines is huge ($256 \times 192 \times 656 \approx 107$), even after 4-time downsampling on the projections.

**TABLE 1. Computation time of the software running on CPU and GPU (in seconds). Step 4 and 6 are not listed due to their negligible computation time.**

| step | 1 | 2 | 3 | 5 | 7 | 8 |
|---|---|---|---|---|---|---|
| CPU (C) | | 600 | | | 2000 | |
| CPU (Matlab) | 7200 | | 16400 | 3300 | | 7200 |
| GPU | 45 | - | 10 | 75 | 720 | 45 |

We accelerate the time-consuming operations (marked with bolded font in Fig.1) on GPU and list the results on the bottom row of Table 1. Since Matlab has lower computation efficiency compared to C language, CUDA C based GPU programming significantly improves the computation efficiency by more than 100 times. For example, step 3 achieves a speedup of around 1600 times since the operation of forward projection is fully parallelizable. Other steps, including FDK reconstruction and the low-pass filtering, also have a substantial decrease in computation time though not as high as forward projection due to their sequential operations. The total computation time of the workflow decreases to about 25 minutes for one iteration. The execution time of noise suppression step using PWLS, however, is only reduced by a factor 3 because the GS solver sequentially updates each pixel value and the parallel computation is only applicable on different views.

### B. COMPARISON WITH THE TRUEBEAM RESULTS

Figs.2 and 3 show the reconstructed CBCT volumes of the phantom and patients without and with the shading correction, the TrueBeam result and the pCT with registration. The scatter artifacts as seen in the images without correction (Fig.2(a) and Fig.3(a)) have been greatly suppressed in our correction (Fig.2(c) and Fig.3(c)) and the TrueBeam results (Fig.2(d) and Fig.3(d)). However, in the results of TrueBeam, shading and streaking artifacts are still visible between the bony structures and the overall spatial uniformity is inferior to that using our software. The residual artifacts could be due to the scatter estimation error of the TrueBeam system, which heavily relies on the accuracy of system modeling.

To quantitatively evaluate the improvement of image quality, five ROIs are selected on the fat/muscle as shown in the axial view of Fig.2(b) and Fig.3(b). One of them is placed where the TrueBeam result has the maximum CT number error and signed with the solid square. The CT numbers of the ROIs are calculated and listed in Table 2 with the errors shown in the parentheses. The proposed method decreases the errors

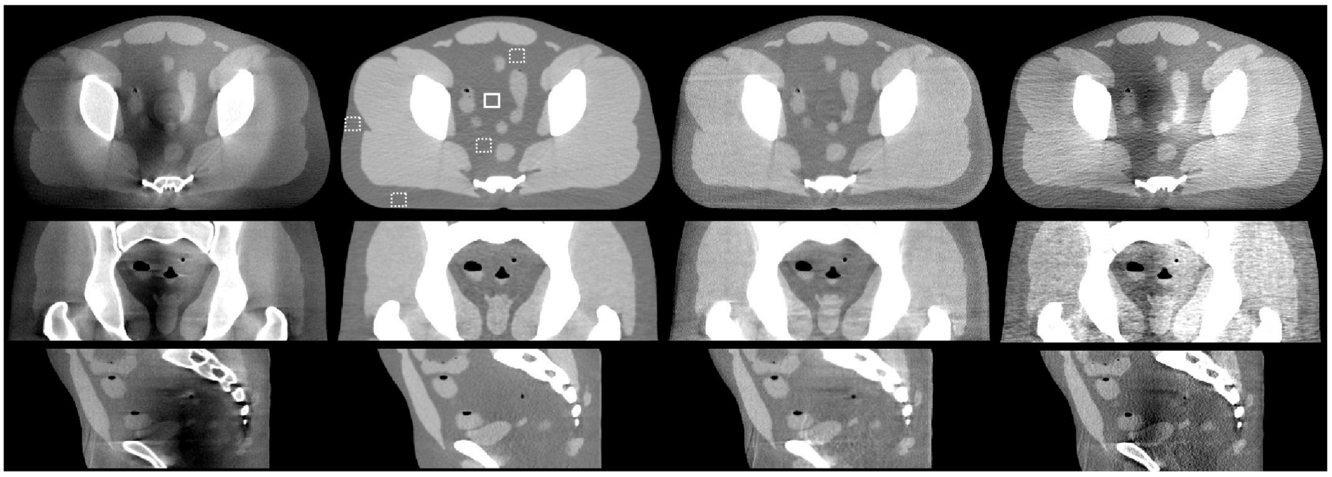


**FIGURE 2.** The pelvis phantom reconstructed image. The display window: [−300 200] HU. The images in the top, middle and bottom row show an axial, coronal and sagittal view, respectively. Column (a): CBCT image without correction; (b): registered pCT; (c): CBCT using the designed software; (d): TrueBeam result. The white squares placed in the axial view of (b) indicate where the overall CT numbers and SNUs are calculated, while the solid one indicates the location where the TrueBeam image has the maximum CT number error.

**TABLE 2.** Comparison of the CT numbers and SNUs of the phantom and patients, measured on the selected ROIs shown in Figs. 2 and 3. The errors of CT number and SNU are listed in the parentheses.

| | No correction | pCT | Proposed | TrueBeam |
|---|---|---|---|---|
| Phantom: | | | | |
| Mean CT number in solid square (HU) | -231 (-190) | -61 | -55 (6) | -137 (-76) |
| Overall CT number (HU) | -168 (-104) | -64 | -60 (4) | -89 (-25) |
| SNU (%) | 24 (22.6) | 1.4 | 3.1 (1.7) | 12.4 (11) |
| Patient #1: | | | | |
| Mean CT number in solid square (HU) | -141 (-126) | 15.3 | 30.0 (15) | 101 (86) |
| Overall CT number (HU) | -217 (-210) | -7.1 | 1.8 (8.9) | 28.8 (36) |
| SNU (%) | 15.3 (12.1) | 3.2 | 4.0 (0.8) | 11.5 (8.3) |
| Patient #2: | | | | |
| Mean CT number in solid square (HU) | -278 (-163) | -115 | -109 (6) | -186 (-71) |
| Overall CT number (HU) | -251 (-116) | -135 | -137 (-2) | -150 (-15) |
| SNU (%) | 14.7 (11.6) | 3.1 | 4.7 (1.6) | 10.0 (6.9) |

of maximum CT number from over 70 HU to below 15 HU compared to the reconstruction of the TrueBeam system and the mean error of the CT number from about 25 HU to below 10 HU. A better spatial uniformity is also achieved by our software. Our method decreases the overall error of the SNU by a factor of around 7.

### C. EFFECTS OF MIS-REGISTRATION

One concern on the pCT-based scatter correction is that our method may carry over too much pCT information and generate false objects on CBCT especially when the registration is inaccurate. To investigate the effects of registration errors on the correction performance, we manually insert a cylindrical rod in the 3D pCT images of the phantom to mimic the patient registration errors between the pCT and CBCT scans and intentionally vary its contrast from 50 to 150 HU as seen on the left column of Fig.4. The corresponding CBCT images with the proposed method were shown in the right column of figure 4. When the contrast is small ($\leq$100 HU), the unmatched rod is not observed in the corrected CBCT images, suggesting that our method faithfully removes the pCT objects that do not exist in the CBCT. As the contrast gets larger (150 HU), some blooming artifact (indicated by the arrows in Fig.4(c)) emerges due to the increased scatter estimation error from the unmatched object. Similar to the results in our previous publications [7], [8], these images indicate that the proposed correction can tolerate registration errors and therefore has an advantage over the existing ''calibration-based'' correction method [12]. This argument is further supported by observing the different soft tissue structures in column (b) and (c) of Fig.3. The proposed method preserves well the outlines of the rectum and the bladder.

## IV. DISCUSSION

In this paper, we develop a software package for quantitative CBCT in radiotherapy using pCT images as the prior information and a statistical noise suppression algorithm. The proposed software has several desired features for clinical applications. First of all, high-quality pCT images of all radiation therapy patients are routinely acquired for treatment planning. Our method utilizes this ''free'' information and requires no hardware modification of current CBCT system. Secondly, the method can be readily built into the image processing workflow of existing kV imager. Thirdly, the method

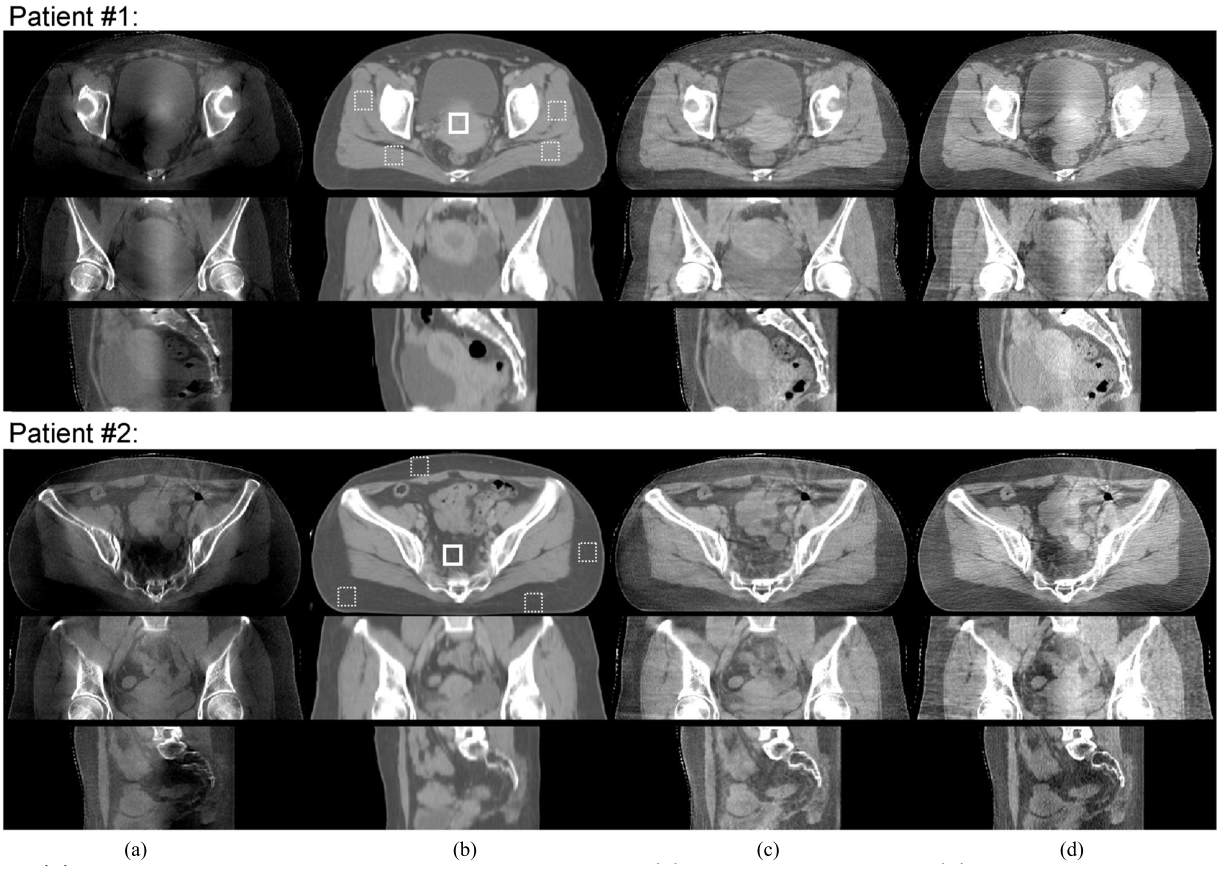


**FIGURE 3.** Reconstructed images of the two pelvis patients. Display window: [−330 170] HU. The figure labels and selected ROIs are similar to those in Fig.2. (a) No correction. (b) Registered pCT. (c) Our correction. (d) From TrueBeam.

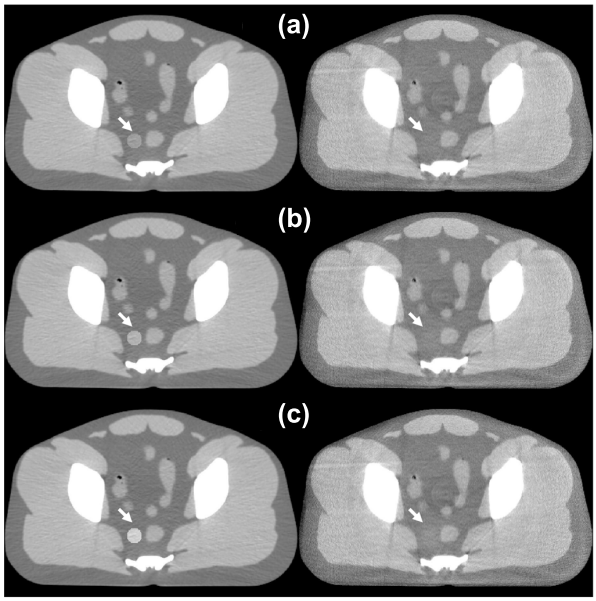


**FIGURE 4.** Proposed correction using pCT images with an unmatched insert of different contrasts. Arrows indicate the positions of the contrast insert. Display window: [−300 200] HU. Left column: pCT images. Right column: CBCT images after the proposed correction. (a) 50 HU. (b) 100 HU. (c) 150 HU.

does not carry over the false geometry information of pCT images onto the corrected CBCT. Finally, the total computation time is reduced to only 25 minutes on a compact GPU workstation, which further facilitates the use of the proposed software in hospitals.

The performance of the proposed framework has been evaluated with pelvis phantom and the pelvis patient on the Varian TrueBeam system. Promising results have been demonstrated in terms of CT number accuracy and spatial uniformity. To completely assess the clinical performance and the utility of our software, more studies are needed to be performed even if we have got the promising results. For example, many of the algorithm parameters, such as the window widths of the low-pass filters and the penalty weight in the noise suppression, are set empirically. Based on more image data, the parameters will be optimized. The performance of the proposed method will be investigated on other part of the body. Using the high-quality CBCT images, we will perform the CBCT-based patient setup and dose calculation, and compare the accuracy to that using pCT.

The computation efficiency of the proposed method can be further improved for an online application. The steps of registration and noise suppression occupy 40% and 48% of current computation time. These two operations can also be further accelerated. For example, plastimatch [31], an open-source GPU-based software package, is suitable for image processing including the registration and segmentation. A different update scheme compatible with parallel computation can be used to shorten the noise suppression process (e.g. the

red-black GS with successive over-relaxation algorithm [32]). Furthermore, multiple GPUs can be applied to speed up the computation as well [33].

## V. CONCLUSION

In this study, we develop an effective software to achieve the scatter correction for quantitative CBCT. The results show a good performance. The computation time is decreased from over 10 hours to below 25 minutes using the parallel computation. The proposed algorithm can reduce the errors of the maximum CT number from over 70 HU to below 15 HU and decrease the errors of the SNU by a factor of around seven compared to the reconstruction on the TrueBeam system. By providing a high quality of CBCT with high efficiency of computation, the promised results may improve the efficiency and accuracy of IGRT.

## ACKNOWLEDGMENT

*(Xiaokun Liang and Yangkang Jiang contributed equally to this work.)*

## REFERENCES

[1] D. Létourneau *et al.*, "Cone-beam-CT guided radiation therapy: Technical implementation," *Radiotherapy Oncol.*, vol. 75, no. 3, pp. 279–286, Jun. 2005.
[2] D. A. Jaffray, J. H. Siewerdsen, J. W. Wong, and A. A. Martinez, "Flat-panel cone-beam computed tomography for image-guided radiation therapy," *Int. J. Radiat. Oncol. Biol. Phys.*, vol. 53, no. 5, pp. 1337–1349, Aug. 2002.
[3] J. H. Siewerdsen and D. A. Jaffray, "Cone-beam computed tomography with a flat-panel imager: Magnitude and effects of X-ray scatter," *Med. Phys.*, vol. 28, no. 2, pp. 220–231, Feb. 2001.
[4] N. Tianye and Z. Lei, "Overview of X-ray scatter in cone-beam computed tomography and its correction methods," *Current Med. Imag. Rev.*, vol. 6, no. 2, pp. 82–89, May 2010.
[5] D. Létourneau *et al.*, "Assessment of residual error for online cone-beam CT-guided treatment of prostate cancer patients," *Int. J. Radiat. Oncol. Biol. Phys.*, vol. 62, no. 4, pp. 1239–1246, Jul. 2005.
[6] M. Guckenberger, J. Meyer, D. Vordermark, K. Baier, J. Wilbert, and M. Flentje, "Magnitude and clinical relevance of translational and rotational patient setup errors: A cone-beam CT study," *Int. J. Radiat. Oncol. Biol. Phys.*, vol. 65, no. 3, pp. 934–942, Jul. 2006.
[7] T. Niu, M. Sun, J. Star-Lack, H. Gao, Q. Fan, and L. Zhu, "Shading correction for on-board cone-beam CT in radiation therapy using planning MDCT images," *Med. Phys.*, vol. 37, no. 10, pp. 5395–5406, 2010.
[8] T. Niu, A. Al-Basheer, and L. Zhu, "Quantitative cone-beam CT imaging in radiation therapy using planning CT as a prior: First patient studies," *Med. Phys.*, vol. 39, no. 4, pp. 1991–2000, Apr. 2012.
[9] L. Zhu, J. Wang, and L. Xing, "Noise suppression in scatter correction for cone-beam CT," *Med. Phys.*, vol. 36, no. 3, pp. 741–752, Mar. 2009.
[10] G. Altorjai *et al.*, "Cone-beam CT-based delineation of stereotactic lung targets: The influence of image modality and target size on interobserver variability," *Int. J. Radiat. Oncol. Biol. Phys.*, vol. 82, no. 2, pp. e265–e272, 2012.
[11] C. Lütgendorf-Caucig, I. Fotina, M. Stock, R. Pötter, G. Goldner, and D. Georg, "Feasibility of CBCT-based target and normal structure delineation in prostate cancer radiotherapy: Multi-observer and image multimodality study," *Radiotherapy Oncol.*, vol. 98, no. 2, pp. 154–161, Feb. 2011.
[12] Y. Yang, E. Schreibmann, T. Li, C. Wang, and L. Xing, "Evaluation of on-board kV cone beam CT (CBCT)-based dose calculation," *Phys. Med. Biol.*, vol. 52, no. 3, pp. 685–705, 2007.
[13] S. Yoo and F.-F. Yin, "Dosimetric feasibility of cone-beam CT-based treatment planning compared to CT-based treatment planning," *Int. J. Radiat. Oncol. Biol. Phys.*, vol. 66, no. 5, pp. 1553–1561, Dec. 2006.
[14] T. Lo, Y. Yang, E. Schreibmann, T. Li, and L. Xing, "Mapping electron density distribution from planning CT to cone-beam CT (CBCT): A novel strategy for accurate dose calculation based on CBCT," *Int. J. Radiat. Oncol. Biol. Phys.*, vol. 63, no. 2, p. S507, 2005.
[15] J. Nijkamp *et al.*, "Adaptive radiotherapy for prostate cancer using Kilovoltage cone-beam computed tomography: First clinical results," *Int. J. Radiat. Oncol. Biol. Phys.*, vol. 70, no. 1, pp. 75–82, Jan. 2008.
[16] Q. J. Wu *et al.*, "On-line re-optimization of prostate IMRT plans for adaptive radiation therapy," *Phys. Med. Biol.*, vol. 53, no. 3, pp. 673–691, 2008.
[17] X. Dong, T. Niu, X. Jia, and L. Zhu, "Relationship between X-ray illumination field size and flat field intensity and its impacts on X-ray imaging," *Med. Phys.*, vol. 39, no. 10, pp. 5901–5909, Oct. 2012.
[18] J. Hsieh, R. C. Molthen, C. A. Dawson, and R. H. Johnson, "An iterative approach to the beam hardening correction in cone beam CT," *Med. Phys.*, vol. 27, no. 1, pp. 23–29, 2000.
[19] H. Li, R. Mohan, and X. R. Zhu, "Scatter Kernel estimation with an edge-spread function method for cone-beam computed tomography imaging," *Phys. Med. Biol.*, vol. 53, no. 23, pp. 6729–6748, 2008.
[20] L. Zhu, N. R. Bennett, and R. Fahrig, "Scatter correction method for X-ray CT using primary modulation: Theory and preliminary results," *IEEE Trans. Med. Imag.*, vol. 25, no. 12, pp. 1573–1587, Dec. 2006.
[21] T. Niu and L. Zhu, "Scatter correction for full-fan volumetric CT using a stationary beam blocker in a single full scan," *Med. Phys.*, vol. 38, no. 11, pp. 6027–6038, Nov. 2011.
[22] L. Zhu, Y. Xie, J. Wang, and L. Xing, "Scatter correction for cone-beam CT in radiation therapy," *Med. Phys.*, vol. 36, no. 6, pp. 2258–2268, 2009.
[23] B. Meng, H. Lee, L. Xing, and B. P. Fahimian, "Single-scan patient-specific scatter correction in computed tomography using peripheral detection of scatter and compressed sensing scatter retrieval," *Med. Phys.*, vol. 40, no. 1, Jan. 2013, Art. no. 011907.
[24] Y. Kyriakou, M. Meyer, and W. A. Kalender, "Technical note: Comparing coherent and incoherent scatter effects for cone-beam CT," *Phys. Med. Biol.*, vol. 53, no. 10, pp. N175–N185, 2008.
[25] T. Niu and L. Zhu, "Single-scan scatter correction for cone-beam CT using a stationary beam blocker: A preliminary study," *Proc. SPIE*, vol. 7961, Mar. 2011, Art. no. 796126.
[26] J. M. Boone, B. A. Arnold, and J. A. Seibert, "Characterization of the point spread function and modulation transfer function of scattered radiation using a digital imaging system," *Med. Phys.*, vol. 13, no. 2, pp. 254–256, Mar. 1986.
[27] L. A. Feldkamp, L. C. Davis, and J. W. Kress, "Practical cone-beam algorithm," *J. Opt. Soc. Amer. A, Opt. Image Sci.*, vol. 1, no. 6, pp. 612–619, 1984.
[28] T. Niu and L. Zhu, "Accelerated barrier optimization compressed sensing (ABOCS) reconstruction for cone-beam CT: Phantom studies," *Med. Phys.*, vol. 39, no. 7, pp. 4588–4598, 2012.
[29] F. Xu and K. Mueller, "Real-time 3D computed tomographic reconstruction using commodity graphics hardware," *Phys. Med. Biol.*, vol. 52, no. 12, pp. 3405–3419, 2007.
[30] R. L. Siddon, "Fast calculation of the exact radiological path for a three-dimensional CT array," *Med. Phys.*, vol. 12, no. 2, pp. 252–255, 1985.
[31] G. C. Sharp, N. Kandasamy, H. Singh, and M. Folkert, "GPU-based streaming architectures for fast cone-beam CT image reconstruction and demons deformable registration," *Phys. Med. Biol.*, vol. 52, no. 19, pp. 5771–5783, 2007.
[32] H. Courtecuisse and J. Allard, "Parallel dense Gauss-Seidel algorithm on many-core processors," in *Proc. 11th IEEE Int. Conf. High Perform. Comput. Commun.*, Jun. 2009, pp. 139–147.
[33] C.-Y. Chou, Y.-Y. Chuo, Y. Hung, and W. Wang, "A fast forward projection using multithreads for multirays on GPUs in medical image reconstruction," *Med. Phys.*, vol. 38, no. 7, pp. 4052–4065, Jul. 2011.

**XIAOKUN LIANG** received the B.S. degree from Southern Medical University, Guangzhou, China. He is currently pursuing the Ph.D. degree with the Shenzhen College of Advanced Technology, University of Chinese Academy of Sciences, Shenzhen, China. He is also a Visiting Student with Stanford University. His research interests focus on medical image analysis, medical physics, and image-guided radiotherapy.

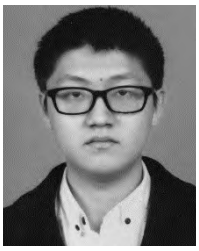

**YANGKANG JIANG** received the B.S. degree from Zhejiang University, Hangzhou, China, where he is currently pursuing the master's degree. His research interests focus on medical image analysis, Monte Carlo simulation, and image-guided radiotherapy.

**YAOQIN XIE** received the B.S., M.S., and Ph.D. degrees from Tsinghua University, Beijing, China, in 1995, 1998, and 2002, respectively. From 2002 to 2010, he was a Lecturer with the School of Physics, Peking University, China. From 2006 to 2008, he was a Research Fellow with the Department of Radiation Oncology, Stanford Medical School, USA. Since 2010, he has been a Full Professor with the Shenzhen Institutes of Advanced Technology, Chinese Academy of Sciences, Shenzhen, China. His research interests include medical image analysis, medical physics, and image-guided radiotherapy.

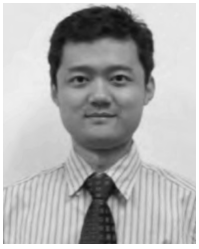

**TIANYE NIU** received the Ph.D. degree from the University of Science and Technology of China, Hefei, China, in 2009. From 2009 to 2013, he held a postdoctoral position in the Medical Physics Program with the Georgia Institute of Technology, GA, USA. He is currently a Full Professor with the Institute of Translational Medicine, Zhejiang University, and also with the Sir Run Run Shaw Hospital, Zhejiang University School of Medicine. His research interests include compressed sensing, low-dose reconstruction, dual-energy CT imaging, spectral CT imaging, IGRT, radiomics, and cone-beam CT instrument.